

## Fe<sub>3</sub>O<sub>4</sub>@ZrO<sub>2</sub>-SO<sub>3</sub>H Nanoparticles: A new magnetically retrievable catalyst for esterification of mono- and dicarboxylic acids

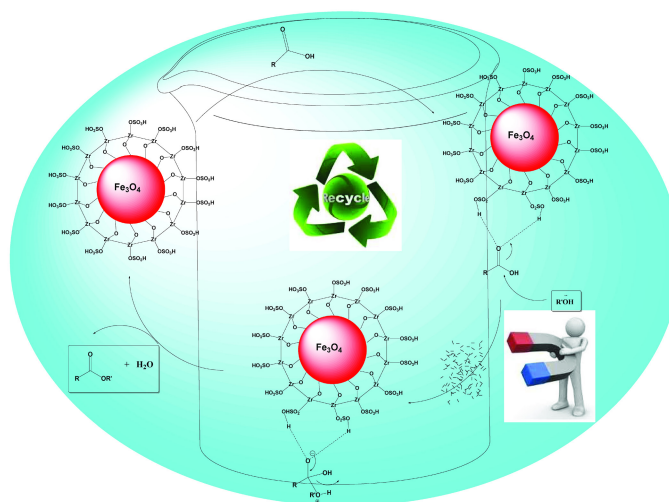
Parya Tayeb Oskoie, Yagoub Mansoori\*

Department of Applied Chemistry, Faculty of Science, University of Mohaghegh Ardabili, Ardabil, Iran

### HIGHLIGHTS

- A zirconia-based magnetic acid catalyst has been prepared.
- Esterification reaction of mono- and dicarboxylic acids by the catalyst has been studied.
- Hammett acidity function has been used for evaluation of the catalyst acidity.

### GRAPHICAL ABSTRACT



### ARTICLE INFO

#### Article history:

Received 31 December 2017

Revised 22 February 2018

Accepted 2 March 2018

#### Keywords:

Fe<sub>3</sub>O<sub>4</sub>@ZrO<sub>2</sub>-supported sulfonic acid

Magnetic acid catalyst

Heterogeneous catalyst

Esterification

### ABSTRACT

In this work preparation of sulfonic acid functionalized magnetite encapsulated zirconia (Fe<sub>3</sub>O<sub>4</sub>@ZrO<sub>2</sub>-SO<sub>3</sub>H) has been reported. Structural, chemical, and magnetic properties of the magnetically supported catalyst have also been investigated by Fourier transform infrared (FT-IR) spectroscopy, wide angle X-ray diffraction spectroscopy (WXR), thermal gravimetric analysis (TGA), energy dispersive X-ray analysis (EDX), transmission electron microscopy (TEM), vibrating sample magnetometer (VSM), Hammett acidity function and pH analysis as well as Brunauer-Emmett-Teller surface area measurement (S<sub>BET</sub>). The esterification reaction of various mono- and dicarboxylic acids with different alcohols was chosen to show the nano-catalytic activity. The reaction conditions were optimized and catalyst recovery was also demonstrated. The magnetic catalyst was magnetically separated and reused several times without significant loss of activity.

\* Corresponding author: Tel.: +9845-31505205 ; Fax: +9845-33514701 ; E-mail address: ya\_mansoori@uma.ac.ir , ya\_mansoori@yahoo.com

DOI: 10.22104/jpsst.2018.2694.1110

## 1. Introduction

Esterification and trans-esterification reactions usually occur in hydrocarbon solvents, such as toluene. Homogeneous acid catalysts, such as sulfuric acid, methane sulfonic acid, *p*-toluene sulfonic acid, and sodium hydrogen sulfate, are the most conventional catalysts used in these reactions. Titanium alkylates and organotin compounds are also used as amphoteric catalysts at elevated temperatures (200 °C) [1]. Corrosion, loss of catalyst, and environment problems produced by acidic wastes are some inevitable characteristics of these catalysts. To minimize waste and atom economy in the use of raw materials, traditional homogeneous acid catalysts have gradually been replaced in recent years by more eco-friendly, sustainable resources and reusable catalysts. Solid acids have many advantages including easy separation of the catalyst from the liquid reaction medium, minimal corrosion, enhanced product selectivity, high catalytic activity, good recyclability, and simple handling requirements [2-5].

Utilization of various supports, such as silica, carbon, and zirconia, have been reported for homogeneous catalysts/reagents [6-9]. In addition, extensive use of organic polymers have also been reported for this purpose [10]. Nevertheless in spite of numerous advantages in some cases, these supports have some common drawbacks which pertain to the traditionally difficult isolation procedure after the completion of reactions, and most importantly the deficient in terms of reusability.

Recently, magnetite-supported catalysts have been considered as suitable alternatives for existing heterogeneous catalysts. Magnetite nanoparticles (MNPs) have been noted for their superparamagnetic property, high coercivity and low Curie temperature [11-15]. Functionalized MNPs exhibit the advantages of biocompatibility, easy recovery by magnetic separation, thermal stability against degradation, large surface area and high capacity of active sites for loading [16]. Easily prepared MNPs are inert, inexpensive, and most importantly, they can be separated magnetically and reused multiple times for the several reaction cycles. They have found wide applications in magnetic recording, drug delivery, adsorption, catalysis, and separation [17-19]. However, they have some drawbacks such as instability in wet air

and monotonous surface characteristic. Furthermore, unmodified MNPs tend to aggregate due to their high specific area and strong inter-particle interaction, which limits their utilization. Therefore, the coating of MNPs by a suitable material with chemical, thermal and mechanical stability which would provide an inert surface layer with compatible surface chemistry for their application of specific targeting is inevitable. For this reason, the development of strategies to coat naked MNPs for stabilization from aggregation over a long period is currently a subject of increasing interest [20].

Among inorganic coating materials silica is widely accepted. The surface chemistry of a silica shell is compatible with various chemicals and bio-molecules for bioconjugation. However, there can be drawbacks in using silica and silica-based materials, including the inability to tolerate high or low pH media and thermal instability. Apart from silica and among other inorganic oxides, zirconia ( $ZrO_2$ ) has been shown to be the most stable metal oxide. It is one of the most widely used ceramic oxides and has many merits in terms of chemical inertness, temperature resistance, high mechanical strength, and chemical properties [21-24]. Core-shells of  $Fe_3O_4@ZrO_2$  are biocompatible, recoverable, and are stable against degradation [25-27].

The use of sulfated zirconia as a heterogeneous catalyst for esterification and/or trans-esterification reactions has been previously reported [28]. In this work, we report the preparation of sulfonic acid functionalized magnetite encapsulated zirconia ( $Fe_3O_4@ZrO_2-SO_3H$ ) as a new magnetically retrievable catalyst for esterification of mono- and di-carboxylic acids. The work originally aimed to simplify the esterification process, deliver easier work-up, cleaner reaction, lower cost, as well as reduce the amount of acidic waste, which is extremely important in terms of environmental and economic considerations. Zirconia was chosen to coat the MNPs due to its improved thermal and chemical stability in comparison with other coating materials, such as silica (as mentioned above). The reactions were cleanly carried out in *p*-toluene as solvent and in the presence of  $Fe_3O_4@ZrO_2-SO_3H$  as the magnetic acid catalyst. Easy reaction conditions, moderate catalytic activity and catalyst recyclability, simple magnetically work-up and lack of acidic waste make  $Fe_3O_4@ZrO_2-SO_3H$  an effective and green catalyst for esterification reactions.

## 2. Experimental

### 2.1. Instruments

The FT-IR (KBr) spectra were recorded on a PerkinElmer RXI spectrophotometer (2 w/w% in KBr, resolution 4  $\text{cm}^{-1}$ , scan no. 6). WXR D spectra were recorded at room temperature on a Philips (X-Pro) X-ray diffractometer using Ni-filtered Cu-K $\alpha$  radiation. The scanning rate was 2°/min over a 2 $\theta$  range of 10–80°. Thermogravimetric analyses (TGA) of the samples were carried out on a Linseis STA PT-1000. The TEM analyses were done on a transmission electron microscope (EM10C, Zeiss) with an acceleration voltage of 80 kV. Ultrasonication was performed using a Dr. Heilscher high intensity ultrasound processor (UP200H, Germany; 13 mm diameter titanium horn, 200 W/cm<sup>2</sup>, 23 kHz). Dispersing of the nanoparticles was done in a Parsonic 7500S ultrasonic bath (PARS NAHAND ENGG. Co., Iran). Magnetization measurements were performed at room temperature using a vibrating sample magnetometer (VSM, 4 inch, Meghnatis Daghigh Kavir Co., Iran) with a maximum magnetic field of 10 kOe. UV-Vis spectra were obtained on a Unico-2100 UV-Vis spectrophotometer. The EDX characterization of the catalyst was performed using a Philips X-30 energy dispersive X-ray spectrometer. The single point N<sub>2</sub> adsorption/desorption analysis according to the BET (Brunauer-Emmett-Teller) method was performed at -196 °C using an automated gas adsorption analyzer (Sibata SA-1100).

### 2.2. Materials

All solvents were of laboratory grade and dried according to procedures described in the literature [29]. The other chemicals were of laboratory grade, obtained from Merck and used without further purification.

### 2.3. Synthesis of MNPs

The synthesis of MNPs was followed by a facile ultrasound assisted method. In a typical procedure, an aqueous solution of ferric chloride (10 ml, 0.6 M) was added to a ferrous sulfate (10 ml, 0.3 M, in HCl 2 M) solution. The mixture was added dropwise into 100 ml of an ammonia solution (0.8 M), while simultaneously sonicating under argon atmosphere for 30 min.

The resulting suspension was cooled down to room temperature and the black precipitate was separated magnetically. The nanoparticles were washed three times with 50 ml portions of ethanol and then dried under vacuum. FT-IR (KBr)  $\nu$   $\text{cm}^{-1}$ : 3406 (br. m), 1629 (w), 586 (s).

### 2.4. Preparation of Nano-Fe<sub>3</sub>O<sub>4</sub>@ZrO<sub>2</sub> Core Shells

Zirconia sol was used to accomplish the modification process, and its preparation was similar to the procedure reported in the literature [30]. Zirconyl chloride octahydrate (1.000 g, 3.10 mmol) was dissolved in 20 ml of a 5:3 (v/v) mixture of ethanol and water and kept at 70 °C for 2 h. Fe<sub>3</sub>O<sub>4</sub> nanoparticles (5.000 g, 21.60 mmol) were added into the zirconia sol, then ultrasonicated for 1 h. After aging for 12 h, the mixture was heated at 300 °C for 2 hrs in a muffle furnace. FT-IR (KBr)  $\nu$   $\text{cm}^{-1}$ : 3423 (br, s), 1629 (w), 728, (s), 637 (s), 586(s).

### 2.5. Preparation of Fe<sub>3</sub>O<sub>4</sub>@ZrO<sub>2</sub>-SO<sub>3</sub>H

Fe<sub>3</sub>O<sub>4</sub>@ZrO<sub>2</sub> nanoparticles (1.000 g) were dispersed in dry CH<sub>2</sub>Cl<sub>2</sub> (50 ml) in an ultrasonic bath for 30 min. Subsequently, chlorosulfonic acid (1.8 ml, 27.03 mmol) was added dropwise to a cooled (ice-bath) dispersion of Fe<sub>3</sub>O<sub>4</sub>@ZrO<sub>2</sub> during 1 h. After the completion of the addition, the mixture was shaken for an additional 6 hs. The resulting Fe<sub>3</sub>O<sub>4</sub>@ZrO<sub>2</sub>-SO<sub>3</sub>H nanoparticles were separated using an external magnet, washed with dry CH<sub>2</sub>Cl<sub>2</sub> and then dried in vacuum. FT-IR (KBr)  $\nu$   $\text{cm}^{-1}$ : 3423 (s), 1629 (m), 1136 (m), 1045 (w), 728, (s), 637 (s), 586 (s).

### 2.6. Esterification of mono- and dicarboxylic acids

In a round-bottom flask equipped with an efficient reflux condenser and a Dean-Stark trap, a mixture of carboxylic acid, alcohol, and the catalyst was refluxed in *p*-toluene for the desired time. The reactions progress was monitored by TLC (petroleum ether/ethylacetate). After completion of the reaction the catalyst was separated magnetically. *p*-Toluene was evaporated under reduced pressure and the residue was dissolved in 5 ml of ethanol. The extent of conversions was calculated by determining the acid numbers (mg KOH/g) of the crude reactions mixture using eq. 1 [28]:

$$\text{Conversion (\%)} = [(a_1 - a_2) \times 100] / a_1 \quad (1)$$

where “ $a_1$ ” is the acid number of the reaction mixture at the beginning (without catalyst), and “ $a_2$ ” is the acid number of the crude reaction mixture after the work-up.

### 3. Results and Discussion

#### 3.1. Preparation of $\text{Fe}_3\text{O}_4@Zr\text{O}_2\text{-SO}_3\text{H}$ nano-catalyst

Magnetite nanoparticles were prepared by the coprecipitation method via Fe(II) and Fe(III) ions. The MNPs were then coated with a zirconia shell to protect the nanoparticles from oxidation and provide reaction sites for further functionalization. Then,  $\text{Fe}_3\text{O}_4@Zr\text{O}_2\text{-SO}_3\text{H}$  nanoparticles were obtained through the reaction of chlorosulfonic acid with  $\text{Fe}_3\text{O}_4@Zr\text{O}_2$ , Scheme 1.

#### 3.2. Characterization of the nano-catalyst

##### 3.2.1. FT-IR Spectral analysis

The FT-IR spectra of  $\text{Fe}_3\text{O}_4$ ,  $\text{Fe}_3\text{O}_4@Zr\text{O}_2$ , and  $\text{Fe}_3\text{O}_4@Zr\text{O}_2\text{-SO}_3\text{H}$  are presented in Figure 1a-c. The band in the region of  $586\text{ cm}^{-1}$  is attributed to the stretching vibration of the Fe–O bond and the bands at about  $637$  and  $727\text{ cm}^{-1}$  belong to the Zr–O–Zr stretching vibrations. The broad band appearing at  $1629\text{ cm}^{-1}$  belongs to the bending vibration of physically adsorbed water molecules. The S=O bond of the sulfonic acid functional group appeared at  $1045$  and  $1136\text{ cm}^{-1}$ . The peak appearing at  $3422\text{ cm}^{-1}$  is related to the stretching vibration of the O–H bond of the  $\text{SO}_3\text{H}$  groups, Figure 1c.

##### 3.2.2. WXR D Analysis

The WXR D patterns of  $\text{Fe}_3\text{O}_4$  and  $\text{Fe}_3\text{O}_4@Zr\text{O}_2\text{-SO}_3\text{H}$

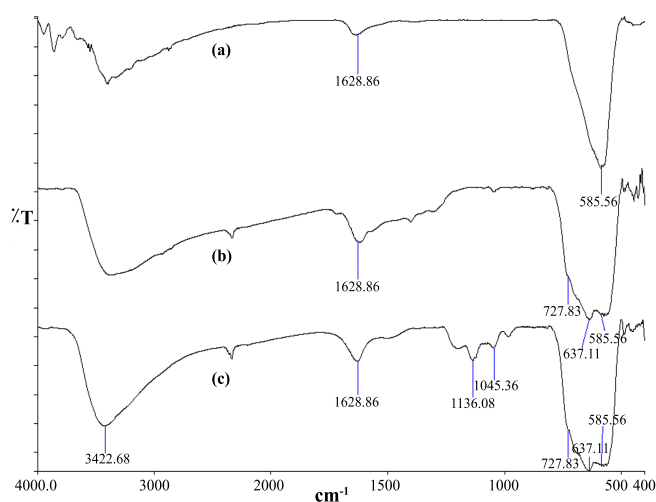
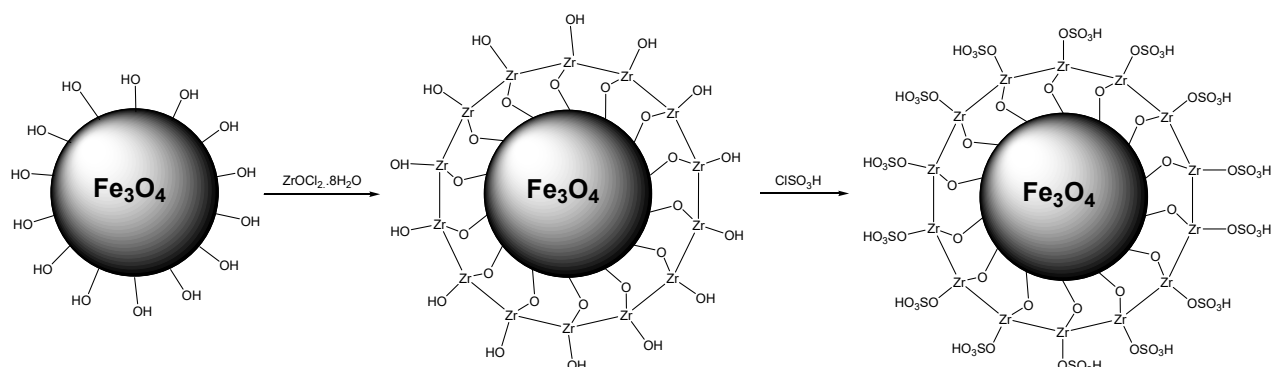


**Fig. 1.** The comparative FT-IR spectra of (a) nano  $\text{Fe}_3\text{O}_4$ ; (b)  $\text{Fe}_3\text{O}_4@Zr\text{O}_2$ ; (c)  $\text{Fe}_3\text{O}_4@Zr\text{O}_2\text{-SO}_3\text{H}$ .

are depicted in Figure 2a-b. The six characteristic peaks correspond to (220), (311), (400), (422), (511) and (440) planes of  $\text{Fe}_3\text{O}_4$  were observed in two samples. These peaks indicate the formation of cubic magnetite nanoparticles (JCPDS-ICDD Copyright 1938, file No. 01-1111) with Fd-3m Space group [31]. The position and the relative intensities of all peaks are consistent with the standard WXR D pattern of  $\text{Fe}_3\text{O}_4$ , confirming retention of the crystalline structure during the functionalization of the MNPs. The average crystallite size  $D$  can be calculated using the Scherrer equation (2):

$$L = K\lambda / \beta \cos\theta \quad (2)$$

where,  $L$  is the coherent length,  $\lambda$  is the wavelength of X-ray radiation ( $\text{Cu}_\alpha=1.54\text{ \AA}$ ),  $\beta$  is the full width at half maxima (FWHM) of the peak and  $\theta$  is the Bragg diffraction angle. In the case of spherical crystallite, it is given by  $L=(3/4)D$  [32]. The average particle size of  $\text{Fe}_3\text{O}_4$  was estimated to be approximately  $21\text{ nm}$ .



**Scheme 1.** Steps for preparation of the  $\text{Fe}_3\text{O}_4@Zr\text{O}_2\text{-SO}_3\text{H}$  nano-catalyst.

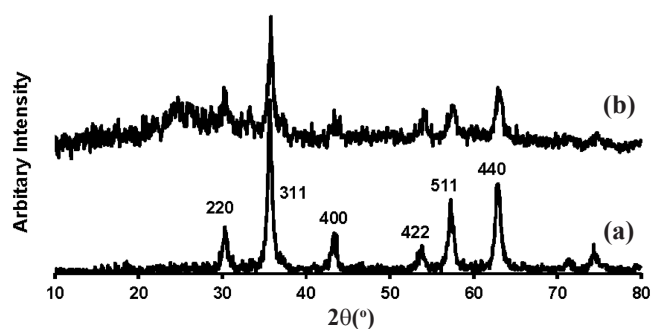


**Fig. 2.** XRD patterns of (a)  $\text{Fe}_3\text{O}_4$  and; (b)  $\text{Fe}_3\text{O}_4@ZrO_2\text{-SO}_3\text{H}$  nanoparticles.

### 3.2.3. TGA Measurements

Figure 3a-c shows the TGA curves of MNPs,  $\text{Fe}_3\text{O}_4@ZrO_2$  and  $\text{Fe}_3\text{O}_4@ZrO_2\text{-SO}_3\text{H}$ . Both MNPs and  $\text{Fe}_3\text{O}_4@ZrO_2$  show a gradual mass loss of approximately 2.74% mass from ambient temperature to 600 °C (Figure 3-a, b), this is related to removing physically adsorbed water molecules (below 200 °C) and surface dehydroxylation in the range of 200-600 °C. In the TGA curve of  $\text{Fe}_3\text{O}_4@ZrO_2\text{-SO}_3\text{H}$  (Figure 3-c), two-stage decomposition is seen corresponding to different mass loss ranges. In the first region, a mass loss of approximately 5.66% mass occurred between 100-330°C, this is related to the removal of  $-\text{SO}_3\text{H}$  groups. Finally, a mass loss of approximately 5.17% mass occurred between 330-600 °C, this is related to the sudden mass loss of sulfonic acid groups [33]. TGA measurement can be used to calculate the amount of sulfonic acid loading [34]. The difference between mass losses of  $\text{Fe}_3\text{O}_4@ZrO_2$  and  $\text{Fe}_3\text{O}_4@ZrO_2\text{-SO}_3\text{H}$  after heating at 600 °C ( $\Delta m = 7.81\%$ ) can be attributed to the multitude of surface sulfonic acid groups. Therefore, sulfonic acid loading (78.1 mg/g of nanoparticles) was estimated from eq. (3).

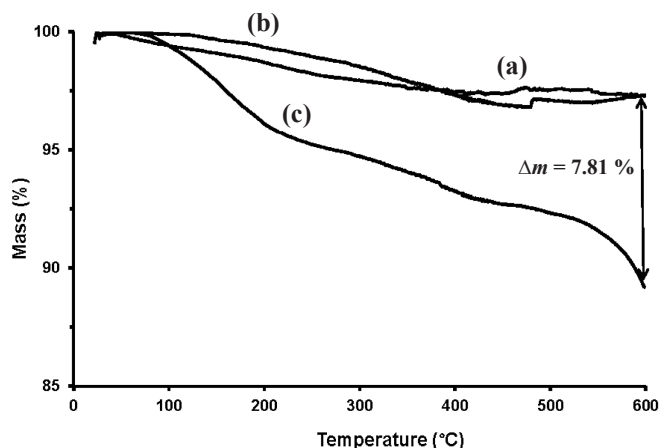


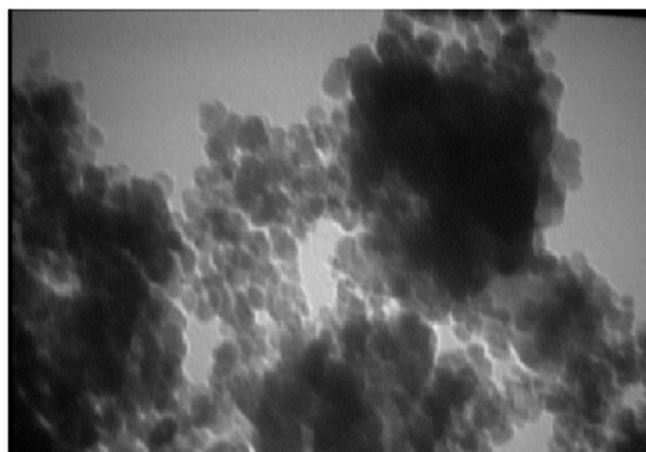
**Fig. 3.** TGA thermograms ( $\text{N}_2$  atmosphere, scan rate of 10 °C/min) of (a) MNPs; (b)  $\text{Fe}_3\text{O}_4@ZrO_2$ ; (c)  $\text{Fe}_3\text{O}_4@ZrO_2\text{-SO}_3\text{H}$ .

$$\text{Sulfonic acid loading (mg/g)} = (\Delta m/100) \times 1000 \quad (3)$$

### 3.2.4. TEM and EDX analysis

The TEM images of MNPs and  $\text{Fe}_3\text{O}_4@ZrO_2\text{-SO}_3\text{H}$  nanoparticles are shown in Figure 4a-b. As observed, MNPs exhibits a uniform spherical shape and has a particle size of approximately 15-20 nm, Figure 4a. This value falls in the size range of a superparamagnetic MNPs that is strongly recommended for in vivo biomedical applications [35,36]. As seen in Figure 4b, the encapsulation of MNPs in the sulfonic acid functionalized zirconia shell produces a diameter of about 5 nm.

X-ray analysis (EDX) of the obtained nano-catalyst by illuminating electron beams on the obtained core-shells reveals the existence of Fe, Zr, S, and O elements, further confirming the formation of the zirconia shell and subsequent functionalization (Figure 5).



(a)

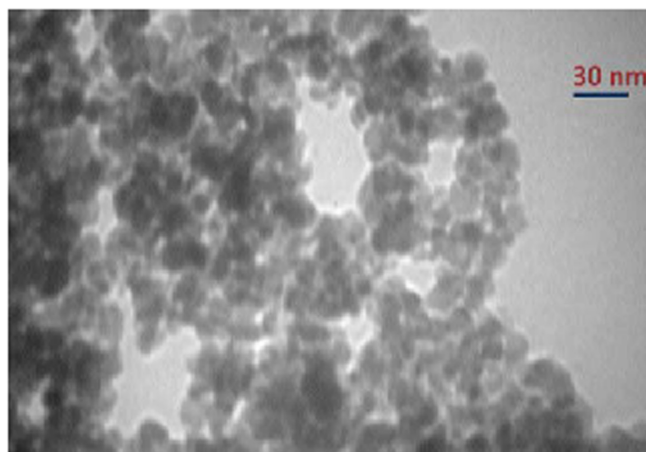


**Fig. 4.** The TEM images of (a)  $\text{Fe}_3\text{O}_4$ ; and (b)  $\text{Fe}_3\text{O}_4@ZrO_2\text{-SO}_3\text{H}$ .

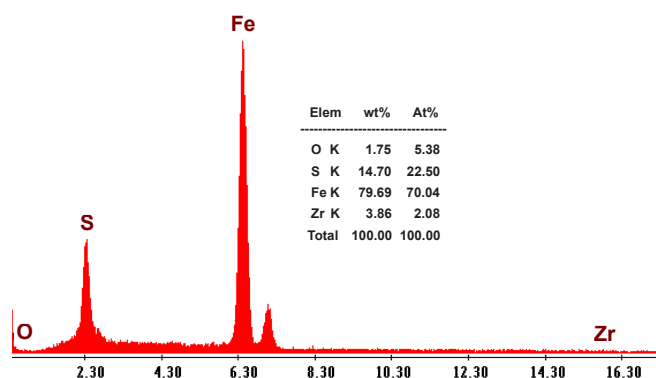


Fig. 5. EDX spectrum of  $\text{Fe}_3\text{O}_4@\text{ZrO}_2\text{-SO}_3\text{H}$ .

### 3.2.5. Magnetization and surface area measurements

The magnetic moment of MNPs,  $\text{Fe}_3\text{O}_4@\text{ZrO}_2$  and  $\text{Fe}_3\text{O}_4@\text{ZrO}_2\text{-SO}_3\text{H}$  were measured over a range of applied fields between 8500 and -8500 Oe at 298 K. The magnetization curves are shown in Figure 6 and the results are summarized in Table 1. The bare  $\text{Fe}_3\text{O}_4$ ,  $\text{Fe}_3\text{O}_4@\text{ZrO}_2$  core-shells and  $\text{Fe}_3\text{O}_4@\text{ZrO}_2\text{-SO}_3\text{H}$  have saturation magnetization values of 61.4, 48.0 and 20.0 emu/g, respectively. The saturation magnetization values are below the reported values for bulk magnetite particles ( $M_s = 92\text{-}100$  emu/g). This may be attributed to the fact that below a critical size, MNPs may exist as a single domain and show the unique phenomenon of superparamagnetism [4,37]. The high magnetization endows the microspheres with fast responsivity in the magnetic separation. The  $M_s$  values clearly show the magnetization is decreased after the coating of  $\text{Fe}_3\text{O}_4$  with  $\text{ZrO}_2$  and then by sulfonic acid loading. This can be attributed to the formation of two non-magnetic coating layers of  $\text{ZrO}_2$  and sulfonic acid on the core-shell structure. The negligible field coercivity of  $\text{Fe}_3\text{O}_4@\text{ZrO}_2\text{-SO}_3\text{H}$  ( $H_c = 0.1$  Oe) shows that the prepared catalyst has superparamagnetic characteristic with the remanence magnetization of  $M_r = 0.2$  emu/g and remanence ratio of  $M_r/M_s = 0.01$ .

**Table 1.** Magnetic properties of MNPs,  $\text{Fe}_3\text{O}_4@\text{ZrO}_2$  and  $\text{Fe}_3\text{O}_4@\text{ZrO}_2\text{-SO}_3\text{H}$ .

Sample	$M_s$ (emu/g) <sup>a</sup>	$M_r$ (emu/g) <sup>b</sup>	$H_c$ (Oe) <sup>c</sup>	$M_r/M_s$ <sup>d</sup>
$\text{Fe}_3\text{O}_4$	61.4	3.20	30.3	0.05
$\text{Fe}_3\text{O}_4@\text{ZrO}_2$	48.0	0.50	9.0	0.01
$\text{Fe}_3\text{O}_4@\text{ZrO}_2\text{-SO}_3\text{H}$	20.0	0.20	0.1	0.01

<sup>a</sup>Saturation magnetization; <sup>b</sup>Remanent magnetization; <sup>c</sup>coercive force; <sup>d</sup>Remanence ratio.

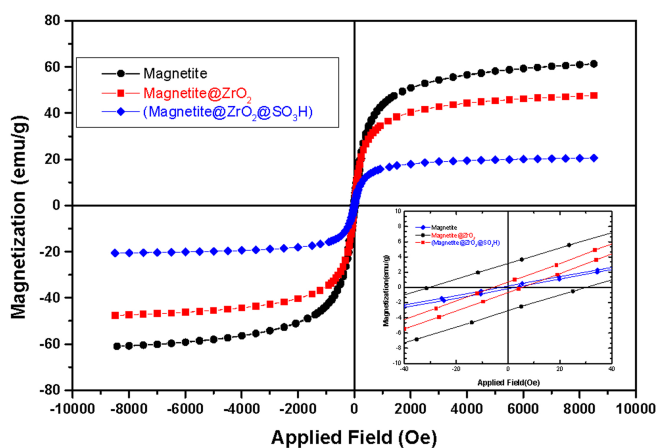


Fig. 6. Magnetization curves for the MNPs,  $\text{Fe}_3\text{O}_4@\text{ZrO}_2$  and  $\text{Fe}_3\text{O}_4@\text{ZrO}_2\text{-SO}_3\text{H}$  at room temperature.

The nanoparticles of catalyst were easily attracted towards the magnet upon application of an external magnetic field, leaving the *p*-toluene solution clear and transparent. It was observed that the catalyst possesses excellent magnetic responsivity and redispersibility, which is an advantage for its applications. Ferromagnetic nanoparticles usually suffer from aggregation upon redispersion, whereas superparamagnetic nanoparticles redisperse in the solution without severe aggregation.

The adsorption characteristics of a material are closely related to its physical morphology. Thus, the surface morphology of  $\text{Fe}_3\text{O}_4@\text{ZrO}_2$  and  $\text{Fe}_3\text{O}_4@\text{ZrO}_2\text{-SO}_3\text{H}$  is an important factor affecting its performance. The specific surface area ( $S_{\text{BET}}$ ) of the obtained nano-particles was measured according to the BET (Brunauer-Emmett-Teller) method, Table 2. As observed,  $\text{Fe}_3\text{O}_4@\text{ZrO}_2\text{-SO}_3\text{H}$  has a lower surface area than  $\text{Fe}_3\text{O}_4@\text{ZrO}_2$ . The main reason for the smaller  $S_{\text{BET}}$  of the coated catalyst compared with the support is due to the anchoring of sulfonic acid species which results in blocking the pores.

### 3.2.6. Acidity of $\text{Fe}_3\text{O}_4@\text{ZrO}_2\text{-SO}_3\text{H}$ nano-catalyst

Hammett acidity function ( $H_0$ ) can effectively express the acidity strength of an acid in organic solvents [38]. It can be calculated using eq. (4).

$$H_0 = pK(I)_{\text{aq}} + \log\left(\frac{[I]_s}{[IH^+]_s}\right) \quad (4)$$

**Table 2.** Measured  $S_{\text{BET}}$  of  $\text{Fe}_3\text{O}_4@\text{ZrO}_2$  and  $\text{Fe}_3\text{O}_4@\text{ZrO}_2\text{-SO}_3\text{H}$ .

Sample	$S_{\text{BET}}$ ( $\text{m}^2/\text{g}$ )
$\text{Fe}_3\text{O}_4@\text{ZrO}_2$	155.9
$\text{Fe}_3\text{O}_4@\text{ZrO}_2\text{-SO}_3\text{H}$	150.4

where,  $[I]_s$  and  $[IH^+]_s$  are the molar concentrations of the unprotonated and protonated forms of the indicator base (4-nitroanilines,  $pK(I)_{aq} = 0.99$ ), respectively. According to the Beer-Lambert Law,  $[I]_s$  and  $[IH^+]_s$  can be calculated using the UV-visible spectrum. In the present experiment,  $CCl_4$  was chosen as the solvent due to its aprotic nature. The  $\lambda_{max}$  of the un-protonated form of the indicator was observed at 330 nm. As shown in Figure 7, the absorbance of the un-protonated form in the presence of  $Fe_3O_4@ZrO_2-SO_3H$  was decreased as compared to the sample of the indicator, which indicated that the indicator was partially protonated. The results are summarized in Table 3, which show the acidity strength of the catalyst. As observed, the Hammett acidity function of  $Fe_3O_4@ZrO_2-SO_3H$  ( $H_0 = 1.47$ ) also supports the synthesis of the acid catalyst with a good density of acid sites ( $-SO_3H$  groups) on the surface.

Sulfonic acid loading was calculated based on the pH analysis of the proton-exchanged brine solutions [5]. Nano-catalyst (0.100 g) was added to an aqueous solution of NaCl (1.0 M, 25 ml) with an initial pH of 5.90 and stirred for 24 hrs. at room temperature. Therefore, the extent of loading (1.99 mmol  $-SO_3H/g$  of acidic catalyst) was measured from the pH of the solution (pH= 2.10) after removing the catalyst with an external magnet. These results in conjunction with the Hammett acidity function ( $H_0$ ) confirm the synthesis of a new catalyst with a good density of acid sites ( $-SO_3H$  groups) on the surface.

### 3.3. Esterification of mono- and dicarboxylic acids by $Fe_3O_4@ZrO_2-SO_3H$

Firstly, in order to find of the optimized amount of the catalyst, a 1:2 molar mixture of phthalic acid and *n*-nonanol was refluxed in *p*-toluene for 12 h (Scheme 2). Different amounts of the catalyst were used and water was removed by a Dean-Stark trap. The reaction progress was follows by TLC (petroleum ether:ethyl

**Table 3.** Calculation of Hammett acidity function ( $H_0$ ) of  $Fe_3O_4@ZrO_2-SO_3H$ .<sup>\*</sup>

Entry	Catalyst	$A_{max}$	$[I]_s$ (%)	$[IH^+]_s$ (%)	$H_0$
1	Blank	0.842	100.0	0.0	-
2	$Fe_3O_4@ZrO_2-SO_3H$	0.631	75.0	25.0	1.47

<sup>\*</sup>Condition for UV-visible spectrum measurement: solvent,  $CCl_4$ ; indicator, 4-nitroaniline ( $pK(I)_{aq} = 0.99$ ),  $3.00 \times 10^{-5}$  mol/L; catalyst,  $Fe_3O_4@ZrO_2-SO_3H$  (10 mg), 25 °C for 24 h.

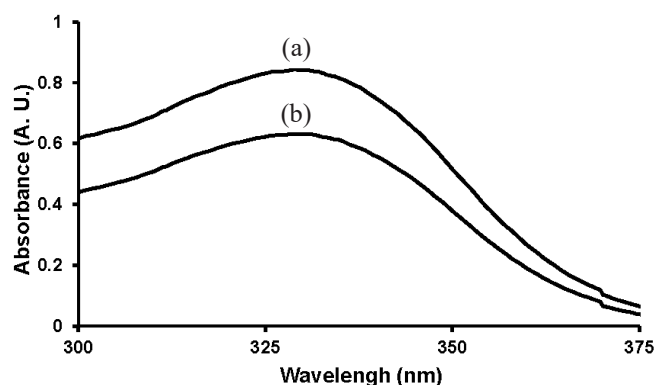
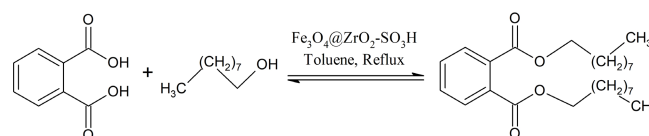


**Fig. 7.** Absorption spectra of (a) 4-nitroaniline (indicator) and (b)  $Fe_3O_4@ZrO_2-SO_3H$  (catalyst) in  $CCl_4$ .

acetate; 85:15) and the results are summarized in Table 4.



**Scheme 2.** Esterification of phthalic acid by *n*-nonanol in the presence of  $Fe_3O_4@ZrO_2-SO_3H$ .

As observed, the reaction does not proceed in the absence of the catalyst (Entry 1), and in the 10 wt% of the total weight of phthalic acid and *n*-nonanol the conversion reached its maximum in 12 h. By screening different amounts of the catalyst, we found that the conversion reaches its maximum when using 10 wt% of the total weight of phthalic acid and *n*-nonanol. This was chosen as the optimum amount of the catalyst for the other esterification reactions. The good catalytic activity of  $Fe_3O_4@ZrO_2-SO_3H$  relates to the sulfonic acid groups of the catalyst, which provide efficient acidic sites.

**Table 4.** Optimization of catalyst amount for the esterification of phthalic acid by *n*-nonanol.<sup>a</sup>

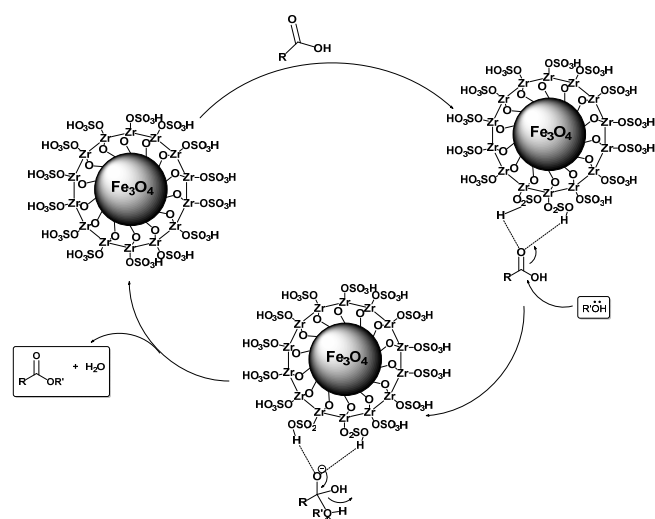
Entry	Catalyst weight (wt%) <sup>b</sup>	Conversion (%) <sup>c</sup>
1	0	30
2	6	58
3	8	70
4	10	83
5	12	85
6	14	86

<sup>a</sup>Reaction conditions: phthalic acid (2 mmol), *n*-nonanol (10 mmol), *p*-toluene (25 ml), reflux for 12 h (followed by TLC). <sup>b</sup>Based on total weight of phthalic acid and *n*-nonanol. <sup>c</sup>Calculated based on acid number measurements.

The capability of  $\text{Fe}_3\text{O}_4@\text{ZrO}_2\text{-SO}_3\text{H}$  toward the esterification of mono- (Table 5) and dicarboxylic acids (Table 6) by different alcohols was also investigated. Most of the prepared compounds are industrially valuable compounds of plasticizers and synthetic ester base lubricants. The FT-IR spectra of the prepared esters and diesters are in accordance with the spectra reported in the Spectral Database for Organic Compounds (SDBS) and reported values in the literature. We could not find any regular relationship between the structures of alcohols and carboxylic acids on one hand and the extent of conversion on the other hand. As a major trend, higher alcohols and long alkyl chain dicarboxylic acids (adipic acid and sebacic acid, Table 5, Entries 14-19) have better reaction yields than that of monocarboxylic acids. This is a positive point, since the diesters of long chain dicarboxylic acids are considered as the base oil for lubricants due to good properties at high and low temperatures, excellent viscosity vs. temperature relationship, low volatility, lubricity, additive solubility, frictional properties, and biodegradability [2,39]. Ethyl esters were obtained in low yields even in the presence of the excess amount of ethanol (ethanol used in and as solvent) due to the low reaction temperature and volatility of EtOH. A possible mechanism for the esterification reaction catalyzed by  $\text{Fe}_3\text{O}_4@\text{ZrO}_2\text{-SO}_3\text{H}$  is proposed as Scheme 3.

### 3.4. Reusability of $\text{Fe}_3\text{O}_4@\text{ZrO}_2\text{-SO}_3\text{H}$ nano-catalyst

For the practical applications of this new magnetic solid acid nanocatalyst, the possibility of magnetic



**Scheme 3.** Proposed reaction pathway for esterification in the presence of  $\text{Fe}_3\text{O}_4@\text{ZrO}_2\text{-SO}_3\text{H}$ .

recycling of the catalyst was also examined. For this purpose, the reaction of phthalic acid and n-nonanol in the presence of  $\text{Fe}_3\text{O}_4@\text{ZrO}_2\text{-SO}_3\text{H}$  was studied. In this procedure, the catalyst was separated from the product after the completion of the reaction by attaching an external magnet, and the conversion was calculated after the work-up. The catalyst was washed with hot dry acetone to remove residual product, then dried and reused in a subsequent reaction. The extent of conversion did not dropped significantly after four reuses of the catalyst. This means that the nature of the nano-catalyst was slightly changed after each run and  $-\text{SO}_3\text{H}$  moieties were tightly anchored with the nano-catalyst. The average extent of the conversion of four consecutive runs was 70%, which clearly demonstrates the practical recyclability of this catalyst (Figure 8).

## 4. Conclusion

The preparation, characterization and use of the  $\text{Fe}_3\text{O}_4@\text{ZrO}_2\text{-SO}_3\text{H}$  nano-catalyst in the esterification reaction of mono- and dicarboxylic acids have been reported. In summary, we showed that the prepared nano-catalyst is an efficient heterogeneous magnetic catalyst for this purpose. Industrial processes will be easier, cleaner, and less complicated when using this catalyst. The catalyst can be readily separated from the reaction mixture magnetically and reused several times without any significant loss of activity. The clean reaction conditions and utilization of a green and magnetically separable heterogeneous catalyst are the main advantages of this catalyst.

## Acknowledgement

The graduate council of the university of Mohagheh Ardabili is gratefully acknowledged for their financial support.

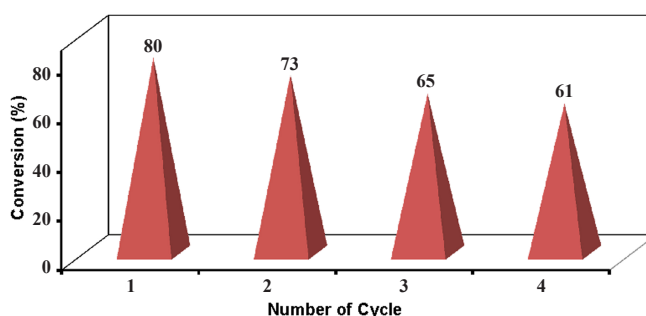


**Fig 8.** Recyclability of  $\text{Fe}_3\text{O}_4@\text{ZrO}_2\text{-SO}_3\text{H}$ .

**Table 5.** Reaction conditions and conversions of monocarboxylic acids by various alcohols.<sup>a</sup>

$$\text{R}-\text{C}(=\text{O})\text{OH} + \text{R}'\text{OH} \xrightleftharpoons[\text{Toluene, Reflux}]{\text{Fe}_3\text{O}_4@\text{ZrO}_2\text{-SO}_3\text{H}} \text{R}-\text{C}(=\text{O})\text{OR}'$$

Entry	Carboxylic Acid	Alcohol	Acid/alcohol molar ratio	Reaction Time (h)	Conversion (%)
1			EtOH solvent	12	0
2			1:3	12	10
3			1:3	12	15
4			1:1	12	10
5			1:3	12	16
6			1:3	12	61
7			1:1	12	25
8			1:3	12	50
9			1:1	12	N.R.
10			1:3	12	57
11			1:1	12	44
12			1:3	12	62
13			EtOH solvent	8	20
14			1:3	12	33

<sup>a</sup>The amount of catalyst was 10 wt% of total weight of carboxylic acid and alcohol.

**Table 6.** Reaction conditions and conversions of dicarboxylic acids by various alcohols.<sup>a</sup>

Entry	Diacid	Alcohol	Diacid/alcohol molar ratio	Reaction Time (h)	Conversion (%)
1			EtOH solvent	8	58
2			1:3	12	7
3			1:3	12	40
4			1:3	12	54
5			1:3	12	63
6			1:3	12	67
7			1:1	8	78
8			1:3	12	83
9			1:1	12	69
10			1:3	12	48
11			EtOH solvent	8	25
12			1:3	12	57
13			1:3	12	60
14			1:3	12	75
15			1:3	12	80
16			1:1	12	76
17			1:3	12	80
18			1:1	12	82
19			1:1	12	75
20			1:1	12	76

<sup>a</sup>The amount of catalyst was 10 wt% of total weight of carboxylic acid and alcohol.

## References

- [1] A. Ross, Industrial applications of organotin compounds, *Ann. N.Y. Acad. Sci.* 125 (1965) 107-123.
- [2] Y. Mansoori, F.S. Tataroglu, M. Sadaghian, Esterification of carboxylic acids by tributyl borate under solvent- and catalyst-free conditions, *Green Chem.* 7 (2005) 870-873.
- [3] Y. Mansoori, F. Tataroglu Seyidov, S. Bohlooli, M.R. Zamanloo, G.H. Imanzadeh, Esterification of carboxylic acids and diacids by trialkyl borate under solvent- and catalyst-free conditions, *Chinese J. Chem.* 25 (2007) 1878-1882.
- [4] Y. Li, T. Leng, H. Lin, C. Deng, X. Xu, N. Yao, P. Yang, X. Zhang, Preparation of Fe<sub>3</sub>O<sub>4</sub>@ZrO<sub>2</sub> core-shell microspheres as affinity probes for selective enrichment and direct determination of phosphopeptides using matrix-assisted laser desorption ionization mass spectrometry, *J. Proteome Res.* 6 (2007) 4498-4510.
- [5] A.R. Kiasat, J. Davarpanah, Fe<sub>3</sub>O<sub>4</sub>@silica sulfuric acid nanoparticles: An efficient reusable nanomagnetic catalyst as potent solid acid for one-pot solvent-free synthesis of indazolo[2,1-b]phthalazine-triones and pyrazolo[1,2-b]phthalazine-diones, *J. Mol. Catal. A- Chem.* 373 (2013) 46-54.
- [6] M.A. Zolfigol, Silica sulfuric acid/NaNO<sub>2</sub> as a novel heterogeneous system for production of thionitrites and disulfides under mild conditions, *Tetrahedron*, 57 (2001) 9509-9511.
- [7] S.T. Firdovski, M. Yagoub, A.E. Parvin, Trans-esterification reaction of dimethyl terephthalate by 2-ethylhexanol in the presence of heterogeneous catalysts under solvent-free condition, *Chinese J. Chem.* 25 (2007) 246-249.
- [8] K. Saravanan, B. Tyagi and H.C. Bajaj, Sulfated zirconia: an efficient solid acid catalyst for esterification of myristic acid with short chain alcohols, *Catal. Sci. Technol.* 2 (2012) 2512-2520.
- [9] A.P. Kumar, J.H. Kim, T.D. Thanh, Y.-I. Lee, Chiral zirconia magnetic microspheres as a new recyclable selector for the discrimination of racemic drugs, *J. Mater. Chem. B*, 1 (2013) 4909-4915.
- [10] N.E. Leadbeater, M. Marco, Preparation of polymer-supported ligands and metal complexes for use in catalysis, *Chem. Rev.* 102 (2002) 3217-3274.
- [11] C. Gómez-Polo, A. Gil, S.A. Korili, J.I. Pérez-Landázabal, V. Recarte, R. Trujillano, M.A. Vicente, Effect of the metal support interactions on the physicochemical and magnetic properties of Ni catalysts, *J. Magn. Magn. Mater.* 316 (2007) e783-e786.
- [12] Z. Wang, D. Wu, G. Wu, N. Yang, A. Wu, Modifying Fe<sub>3</sub>O<sub>4</sub> microspheres with rhodamine hydrazide for selective detection and removal of Hg<sup>2+</sup> ion in water, *J. Hazard. Mater.* 244-245 (2013) 621-627.
- [13] M.B. Gawande, A.K. Rathi, I.D. Nogueira, R.S. Varma, P.S. Branco, Magnetite-supported sulfonic acid: a retrievable nanocatalyst for the Ritter reaction and multicomponent reactions, *Green Chem.* 15 (2013) 1895-1899.
- [14] H. Naeimi, Z. Nazifi, A highly efficient nano-Fe<sub>3</sub>O<sub>4</sub> encapsulated-silica particles bearing sulfonic acid groups as a solid acid catalyst for synthesis of 1,8-dioxo-octahydroanthene derivatives, *J. Nanopart. Res.* 15 (2013) 2026-2037.
- [15] A. Mobaraki, B. Movassagh, B. Karimi, Magnetic solid sulfonic acid decorated with hydrophobic regulators: A combinatorial and magnetically separable catalyst for the synthesis of  $\alpha$ -aminonitriles, *ACS Comb. Sci.* 16 (2014) 352-358.
- [16] A. Mobaraki, B. Movassagh, B. Karimi, Hydrophobicity-enhanced magnetic solid sulfonic acid: A simple approach to improve the mass transfer of reaction partners on the surface of the heterogeneous catalyst in water-generating reactions, *Appl. Catal. A-Gen.* 472 (2014) 123-133.
- [17] I. Chourpa, L. Douziech-Eyrolles, L. Ngaboni-Okassa, J.-F. Fouquenot, S. Cohen-Jonathan, M. Souce, H. Marchais, P. Dubois, Molecular composition of iron oxide nanoparticles, precursors for magnetic drug targeting, as characterized by confocal Raman microspectroscopy, *Analyst*, 130 (2005) 1395-1403.
- [18] M. Shokouhimehr, Y. Piao, J. Kim, Y. Jang, T. Hyeon, A magnetically recyclable nanocomposite catalyst for olefin epoxidation, *Angew. Chem. Int. Edit.* 46 (2007) 7039-7043.
- [19] S. Laurent, D. Forge, M. Port, A. Roch, C. Robic, L. Vander Elst, R.N. Muller, Magnetic iron oxide nanoparticles: synthesis, stabilization, vectorization, physicochemical characterizations, and biological applications, *Chem. Rev.* 108 (2008) 2064-2110.
- [20] V.V. Costa, M.J. Jacinto, L.M. Rossi, R. Landers,

- E.V. Gusevskaya, Aerobic oxidation of monoterpenic alcohols catalyzed by ruthenium hydroxide supported on silica-coated magnetic nanoparticles, *J. Catal.* 282 (2011) 209-214.
- [21] J. Nawrocki, M. Rigney, A. McCormick, P.W. Carr, Chemistry of zirconia and its use in chromatography, *J. Chromatogr. A*, 657 (1993) 229-282.
- [22] C.J. Dunlap, P.W. Carr, C.V. McNeff, D. Stoll, Peer Reviewed: Zirconia stationary phases for extreme separations, *Anal. Chem.* 73 (2001) 598 A-607 A.
- [23] Z.-G. Shi, L. Xu, S.-L. Da, Y.-Q. Feng, Study of the magnesia additive on the characterization of zirconia–magnesia composite sphere, *Micropor. Mesopor. Mat.* 94 (2006) 34-39.
- [24] J.S. Moya, S. Lopez-Esteban, C. Pecharromán, The challenge of ceramic/metal microcomposites and nanocomposites, *Prog. Mater. Sci.* 52 (2007) 1017-1090.
- [25] J. Randon, S. Huguet, A. Piram, G. Puy, C. Demesmay, J.-L. Rocca, Synthesis of zirconia monoliths for chromatographic separations, *J. Chromatogr. A*, 1109 (2006) 19-25.
- [26] A.P. Kumar, J.H. Park, Fast separations of chiral  $\beta$ -blockers on a cellulose tris(3,5-dimethylphenylcarbamate)-coated zirconia monolithic column by capillary electro-chromatography, *J. Chromatogr. A*, 1218 (2011) 5369-5373.
- [27] A.P. Kumar, J.H. Park, Zirconia-based stationary phases for chiral separation: Mini Review, *Anal. Lett.* 45 (2012) 15-42.
- [28] F.T. Sejidov, Y. Mansoori, N. Goodarzi, Esterification reaction using solid heterogeneous acid catalysts under solvent-less condition, *J. Mol. Catal. A-Chem.* 240 (2005) 186-190.
- [29] W.L.F. Armarego, C.L.L. Chai, Purification of laboratory chemicals, 6<sup>th</sup> ed., Butterworth-Heinemann, Elsevier Inc., Burlington, 2009.
- [30] Y.-W. Wu, J. Zhang, J.-F. Liu, L. Chen, Z.-L. Deng, M.-X. Han, X.-S. Wei, A.-M. Yu, H.-L. Zhang,  $\text{Fe}_3\text{O}_4@\text{ZrO}_2$  nanoparticles magnetic solid phase extraction coupled with flame atomic absorption spectrometry for chromium(III) speciation in environmental and biological samples, *Appl. Surf. Sci.* 258 (2012) 6772-6776.
- [31] J.D. Hanawalt, H.W. Rinn, L.K. Frevel, Chemical Analysis by X-Ray Diffraction, *Ind. Eng. Chem. Anal. Ed.* 10 (1938) 457-512.
- [32] A. Guinier, X-ray diffraction: in crystals, imperfect crystals, and amorphous bodies. Courier Dover Dover Publications, New York, 2013.
- [33] A. Amoozadeh, S. Rahmani, M. Bitaraf, F.B. Abadi, E. Tabrizian, Nano-zirconia as an excellent nano-support for immobilization of sulfonic acid: a new, efficient and highly recyclable heterogeneous solid acid nanocatalyst for multicomponent reactions, *New J. Chem.* 40 (2016) 770-780.
- [34] Y. Mansoori, T. Mohseni Masooleh, Polyimide/organo-montmorillonite nanocomposites: A comparative study of the organoclays modified with aromatic diamines, *Polym. Composite.* 36 (2015) 613-622.
- [35] H. Cao, J. He, L. Deng, X. Gao, Fabrication of cyclodextrin-functionalized superparamagnetic  $\text{Fe}_3\text{O}_4$ /amino-silane core-shell nanoparticles via layer-by-layer method, *Applied Surface Science*, 255 (2009) 7974-7980.
- [36] M. Pooresmaeil, Y. Mansoori, M. Mirzaeinejad, A. L. I. Khodayari, Efficient removal of methylene blue by novel magnetic hydrogel nanocomposites of poly(acrylic acid), *Adv. Polym. Tech.* 37 (2016) 262-274.
- [37] J. Choubey, A.K. Bajpai, Investigation on magnetically controlled delivery of doxorubicin from superparamagnetic nanocarriers of gelatin crosslinked with genipin, *J. Mater. Sci.-Mater. M.* 21 (2010) 1573-1586.
- [38] H. Xing, T. Wang, Z. Zhou, Y. Dai, The sulfonic acid-functionalized ionic liquids with pyridinium cations: Acidities and their acidity-catalytic activity relationships, *J. Mol. Catal. A-Chem.* 264 (2007) 53-59.
- [39] G. Van der Waal, Ester base fluids, Unichem International, Gouda, The Netherlands, 1995.